Non-destructive 3D exploration of silicate glass corrosion: a combined multiscale approach from the macro to the nanoscale

Giulia Franceschin,*[a] Roberta Zanini,[a] Gianluca Iori,[b] Elena Longo,[c] Giorgio Divitini,[d] Giuliana Tromba,[c] and Arianna Traviglia[a]

a. Center for Cultural Heritage Technologies (CCHT), Istituto Italiano di Tecnologia, Epsilon building, via Torino 155, Venice, 30170, Italy
b. SESAME - Synchrotron-light for Experimental Science and Applications in the Middle East, Allan 19252, Jordan
c. Elettra - Sincrotrone Trieste S.C.p.A., AREA Science Park, 34149 Basovizza, Trieste, 34149, Italy
d. Electron Spectroscopy and Nanoscopy, Istituto Italiano di Tecnologia, Via Morego 30, Genoa, 16163, ItalyKEYWORDS Glass corrosion, silica nanoparticles, X-ray micro-computed tomography, iridescence, multi-layer structure, multi-scale analysis.

Supplementary Text

Sample details

Aquileia's strategic location at the intersection of major Roman roads and waterways made it a thriving centre for trade and commerce. Founded in 181 B.C. as a military colony near the Adriatic Sea, the city grew in significance over time. Its advantageous position allowed for easy transportation of goods by both land and water, attracting merchants and traders from different regions. The archaeological research conducted in Aquileia over the last two hundred years have revealed a vast array of artefacts, including a significant number of glass objects.[1,2] These discoveries provide valuable insights into the historical importance of Aquileia as a centre for glass production and distribution.

The analysed glass shard was found with approximately 280 other glass fragments, but it was the only one presenting the distinguished shimmery patina, while the others had common iridescent patinas observed on ancient glass. The fragment was found on the topsoil in an agricultural field, most likely uncovered because of recent field ploughing activities.

The discovery location corresponds to the final segment of an ancient Roman canal (now buried) that once connected Aquileia to a nearby marshland and the Adriatic Sea (*Anfora* canal). This area, which underwent significant changes over the centuries, was reclaimed during the 18th and 19th centuries.

The soil in the surroundings of Aquileia is characterised as stratified, consisting of layers with varying thickness and composition.[3] The top layer, associated with the modern period, is often composed of organic matter. Directly beneath that layer, at a depth of 1-2 meters, lies a layer typically composed of a mixture of sand, silt, and clay, which corresponds to the Roman period. The soil properties in Aquileia have been identified as favourable for the preservation of both organic materials (such as wood and textiles) as well as inorganic ones (like glass and ceramics).[4] In the present day, at the site where the sample was discovered, the soil is clay-rich and wet, with a slightly acidic pH and a high cation exchange capacity.[5]

In a previous study,[6] the sample was identified as a fragment of a Roman glass object using laser ablation - inductively coupled plasma - mass spectroscopy (LA-ICP-MS). This analysis revealed that the unaltered core of the glass had a silica-soda-lime high-magnesium (HMG) composition. The presence of a high concentration of Fe, as indicated by the analysis, suggested that the original colour of the glass was dark green. It is likely that Fe-rich sand and plant ashes were added to the glass batch as a reducing agent to achieve this colour. The same study also reported on the composition and the distribution of elements within the alteration patina of the sample, which was correlated to the specific soil composition in the area where it was found.

Binary mask generation

The binary mask of the alteration pit is obtained following these steps:

1. A cylindrical mask of the reconstruction volume (BW_circle) is selected as voxels with grey value different than 0.
2. The altered glass (BW_pit) is segmented based on the image grey values using one lower and one upper threshold that are manually selected.
3. All unconnected clusters of voxels are removed.
4. A mask is computed as ~(BW_pit | BW_circle). This includes the unaltered glass, voids, and secondary phases with high image intensity within the pit.
5. The largest region (unaltered glass) is removed from it, leaving only voids and secondary phases within the pit.
6. The mask obtained in this way is merged to BW_pit, closing most voids within the pit region.
7. Further image opening followed by a holes filling step are applied to BW_pit.
8. The obtained 3D pit mask is finally inspected using Dragonfly, removing manually the remaining protrusions and voids.

A mask of the alteration front is obtained as the edge of the masked pit. Secondary phases are segmented applying a single lower threshold that is manually selected.

Analysis of secondary alteration phases

For the particle analysis of secondary alteration phases a copy of the pit mask is modified manually by removing one side of the pit U-shape where the alteration front has detached from the glass bulk. Similarly, particles within the central void of the pit are disregarded. This is done to exclude areas where the regular layered structure has been disrupted or substituted by substantial portions of air and soil.

Individual secondary phase particles are labelled in 3D and their volume, sphericity, principal radii, centre of mass, and 3D orientation are calculated using the spam Python toolkit. Plots of grains orientation are obtained projecting their orientation vector on the SX-µCT slice plane. The grain degree of anisotropy is calculated as the ratio between major and minor axes of an ellipsoid fitting the particle. Distance transforms of the alteration front and voids masks are used to interpolate the distance between labelled phases and (i) pit front or (ii) air-filled voids, respectively.

Optical microscopy

Optical microscopy observations performed on multiple areas of our sample highlighted the presence of a multi-layered lamellar structure developing parallel to the interface between altered and unaltered glass (red dashed line in Figure S1a) In the confined space inside pits, the filling material is visible as an organised sequence of multiple alternating (Figure S1) layers of white, yellow, and orange colour. Grains of secondary phases are visible as brown-red spots within the alteration layers inside the major pit, as depicted in Figure 4b, which displays the layers' cross-section sequence, as well as in the surface layers, sandwiched between different lamellae blocks (as seen in planar direction in Figure S1c). This correspondence indicates once again that the altered glass has a similar composition and structure both on the sample surface and inside the pits. We hypothesised that these brown-red grains are the same visible as bright particles of highly X-ray attenuating material observed with SX-µCT analysis.

Compositional analysis of surface and pit patina

To understand the chemical composition of the particles of secondary phases present on the sample's surface and inside pits, we conducted a multi-technique analysis directly inside the major pit and on layers collected from the surface patina. The study, which included STEM coupled with Energy-dispersive X-ray (STEM-EDXS) spectroscopy, revealed that the thin lamellae inside the patina on the surface region are composed almost exclusively of Si and O, with some inclusion of Fe (Figure S3a). Furthermore, micro-Raman spectroscopy of the white layers inside the pit indicated the presence of amorphous silica as the main component (Figure S3b), similarly to the composition of the surface patina. The presence of brown-red grains in the pit area is responsible for the detection of hematite bands in the Raman spectrum (Figure S3c). However, these grains undergo rapid colour variation when exposed to the 785 nm laser beam of the instrument, inducing a material transformation to the crystalline hematite state which is detected. Such a phase transformation under the influence of a laser power of 1mW or more is known to occur for many iron minerals, especially when the material under analysis has low crystallinity.[7] Due to this transformation, Raman spectroscopy does not allow the identification of the original phase constituting the brown-red grains, but only of a by-product derived from the laser-induced alteration. Nonetheless, the presence of Fe is verified.

Supplementary figures

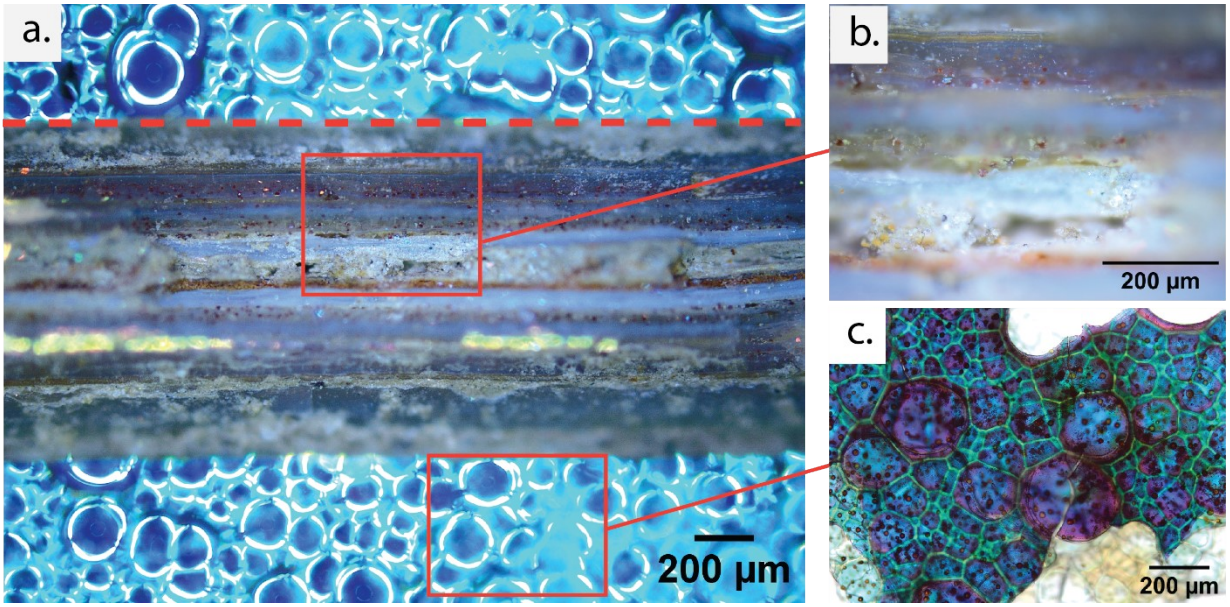

Figure S1. (a) Dark-field optical image of the area containing the analysed pit and the shimmery alteration patina, the red dashed line representing the interface between unaltered glass and alteration layers. (b) Detail of the inner structure of the pit filled with longitudinally organised material; (c) transmitted light optical image of multiple layers of surface lamellae with different colour shades in relation to the number of overlapping layers and grains of secondary phase embedded in it.

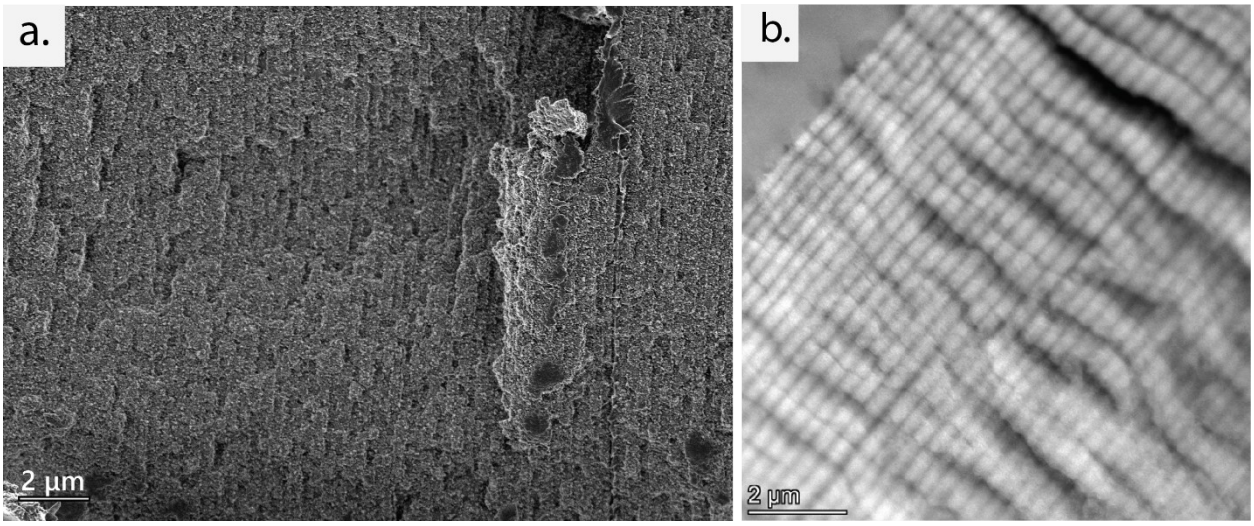

Figure S2. (a) SEM secondary electron image of a block of multiple thin lamellae from the surface patina made of aggregated nanoparticles (NPs). (b) STEM image of the stacked lamellae building the patina layers.

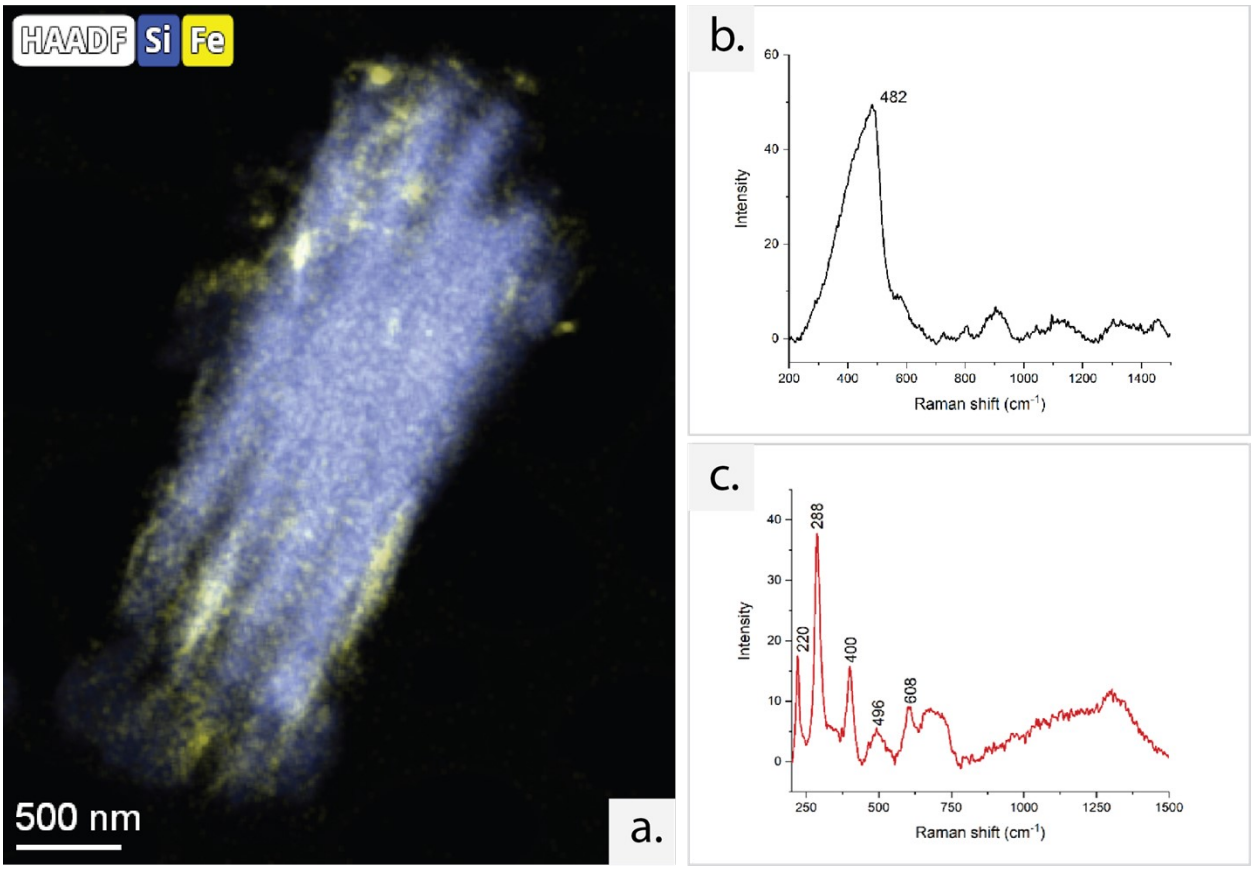

Figure S3. (a) Overlay of STEM-HAADF image, Si and Fe chemical maps from STEM-EDX collected on a fragment of surface patina. (b) Raman spectra of amorphous silica and (c) iron-rich species in the layers inside the major pit.

Supplementary references

1 D. D. Martino, E. Gagetti, G. Marcuccci, Q. Lemasson and M. P. Riccardi, *J. Phys.: Conf. Ser.*, 2022, **2204**, 012074.

2 D. Whitehouse, *Journal of Roman Archaeology*, 2006, **19**, 538–539.

3 G. Arnaud-Fassetta, M.-B. Carre, R. Marocco, F. Maselli Scotti, N. Pugliese, C. Zaccaria, A. Bandelli, V. Bresson, G. Manzoni, M. Montenegro, C. Morhange, M. Pipan, A. Prizzon and I. Siché, *Géomorphologie : relief, processus, environnement*, 2003, **9**, 227–245.

4 M. Kibblewhite, G. Tóth and T. Hermann, *Science of The Total Environment*, 2015, **529**, 249–263.

5 S. Toniolo, *Soil characterisation to investigate the role of burial environment in archaeological glass alteration*.

6 G. Guidetti, R. Zanini, G. Franceschin, M. Moglianetti, T. Kim, N. Cohan, L. Chan, J. Treadgold, A. Traviglia and F. G. Omenetto, *Proceedings of the National Academy of Sciences*, 2023, **120**, e2311583120.

7 M. Hanesch, *Geophysical Journal International*, 2009, **177**, 941–948.